The Astronomical Journal, 127:1784–1790, 2004 March

THE NUCLEUS OF COMET 48P/JOHNSON

David Jewitt[1] and Scott Sheppard[1]
Institute for Astronomy, University of Hawaii, 2680 Woodlawn Drive, Honolulu, HI 96822-1897; jewitt@ifa.hawaii.edu, sheppard@ifa.hawaii.edu
Received 2003 August 11; accepted 2003 December 11

ABSTRACT

We present new observations of short-period (Jupiter family) comet 48P/Johnson taken over several months when near ∼4 AU heliocentric distance. CCD photometry shows that this object has a pointlike inner surface brightness profile. It varies cyclically in brightness, with a light-curve period 14.50 ± 0.02 hr and photometric range $\Delta m_R = 0.32 \pm 0.05$ mag. We attribute these variations to the rotation of a bare, aspherical nucleus with projected semiaxes 3.0×2.2 km (0.04 albedo assumed) and (two-peaked) rotation period 29.00 ± 0.04 hr. The phase coefficient of the nucleus is 0.059 ± 0.002 mag deg^{-1}, consistent with a low-albedo surface. A faint tail is evident in a deep composite image but appears to contribute little to the nucleus signal.

Key words: comets: general — comets: individual (48P/Johnson) — Kuiper belt

1. INTRODUCTION

The nuclei of comets are most usually observed in the presence of near-nucleus comae, produced by the sublimation of volatiles in response to the heat of the Sun. Although not optically thick, the scattering cross section of the matter in the coma can easily exceed that of the nucleus itself. As a result, few cometary nuclei have been studied directly, and the ensemble properties of these bodies are not well known. Scientifically, the nuclei deserve attention because they are potentially some of the closest links we possess to the solar system's initial conditions. The Jupiter-family comets, of which 48P/Johnson is a typical example, are thought to have been recently (median time $\sim 10^7$ yr) dislodged from the Kuiper belt (Tiscareno & Malhotra 2003). They have been stored at low temperatures ($T \leq 50$ K) since their accretion in the protoplanetary disk of the Sun, 4.5 Gyr ago, and may preserve volatiles and other materials from that epoch. On the other hand, recent observations have uncovered differences in the surface colors (Jewitt 2002) and shapes (Jewitt, Sheppard, & Fernández 2003) of the cometary nuclei that are most likely evolutionary in nature, while it has long been recognized that the spins of the cometary nuclei are influenced by outgassing torques. The present state of knowledge is such that we do not yet understand either the initial conditions of the cometary nuclei or the processes of modification that have occurred following their injection into the inner solar system.

Comet 48P/Johnson was discovered in 1949 (Johnson 1949). With current semimajor axis $a = 3.64$ AU, eccentricity $e = 0.3666$ and inclination $i = 13\overset{\circ}{.}6$, and a Tisserand invariant $T_J = 2.98$, it is firmly classified as a member of the Jupiter family of comets (the JFCs). The perihelion distance is $q \sim 2.3$ AU, while aphelion at $Q \sim 4.97$ AU allows the comet to interact strongly with Jupiter. However, no strong interactions have been identified from backward integrations of the equations of motion to about 1600 A.D. (Carusi et al. 1985). It was last observed postperihelion in 1998 at heliocentric distance $R = 3.36$ AU, by Lowry & Fitzsimmons (2001). They detected a strong coma and set a limit to the effective nucleus radius $r_e \leq 3.5$ km (albedo $p_R = 0.04$ assumed).

2. OBSERVATIONS

Time-series photometric observations were taken at the University of Hawaii (UH) 2.2 m telescope atop Mauna Kea, Hawaii, where a Tektronix 2048×2048 pixel CCD camera was used at the f/10 focus of the telescope. The image scale was $0\overset{''}{.}219$ pixel^{-1}. Images were taken through a broadband Mould *R* filter. We mostly tracked the telescope at nonsidereal rates while autoguiding on nearby stars. On a few occasions, because of technical and other problems, we took data without use of the guider. Integration times were limited to 300 s in order to minimize the motion of the comet relative to the fixed stars and to maintain high time resolution in the event that the comet might rotate rapidly. A journal of observations is given in Table 1.

Internal calibration of the data was obtained by subtracting a bias signal, determined for each image from an overclocked region of the CCD, and then by dividing by a flat-field image. The latter was obtained from a median combination of images of the twilight sky. Absolute photometric calibration was secured from repeated observations of standard stars near in the sky to the comet and interleaved in time with the comet observations (Landolt 1992). Subsequent measurements of the standard stars proved consistent roughly at the ±0.01 mag level. Measurements of the comet are individually less certain because of the increased effects of sky noise and background uncertainty on this fainter target.

Observations at the 10 m Keck I Telescope employed the LRIS imaging camera (Oke et al. 1995). The LRIS camera uses an inclined dichroic filter to separate the light into blue and red channels that can be observed simultaneously, with the dividing wavelength $\lambda = 5600$ Å. The red channel has an image scale of $0\overset{''}{.}22$ pixel^{-1}. Images were flattened in much the same way as at the UH telescope, except that we used dome flats instead of twilight flats for the *R*-filter data. Calibration was again secured using the Landolt standard stars.

For the light-curve observations that form the bulk of the data presented here, we measured the brightness of 48P relative to background stars in order to provide protection against apparent fluctuations caused by variable image quality and atmospheric

[1] Guest Observer at the W. M. Keck Observatory, which is operated as a scientific partnership among the California Institute of Technology, the University of California, and the National Aeronautics and Space Administration. The Observatory was made possible by the generous financial support of the W. M. Keck Foundation.

TABLE 1
JOURNAL OF OBSERVATIONS

UT Date (2003)	Tel.[a]	R[b] (AU)	Δ[c] (AU)	α[d] (deg)
Feb 25	UH	3.981	3.371	12.2
Feb 26	UH	3.978	3.355	12.1
Mar 2	UH	3.966	3.296	11.4
Mar 3	UH	3.964	3.281	11.4
Mar 4	UH	3.961	3.267	11.3
Mar 5	UH	3.958	3.253	11.2
Apr 1	UH	3.876	2.951	6.4
Apr 2	UH	3.873	2.943	6.2
Apr 3	UH	3.870	2.936	6.1
May 27	Keck	3.700	2.943	11.7
Jul 2	UH	3.581	3.267	16.2

[a] University of Hawaii 2.2 m telescope or Keck 10 m telescope, both located on Mauna Kea.
[b] Heliocentric distance.
[c] Geocentric distance.
[d] Phase angle.

extinction variations. The skies were clear for all observations, and the median image quality (including effects due to the atmosphere, the telescope optics, and sidereal tracking errors in the telescope) was 0.″8 FWHM. The motion of the comet within the ~250 s integration period was ~0.″7 in the February and March data, comparable to the image quality. Experiments showed that photometric apertures 10 pixels (2.″19) in radius were large enough to make an accurate comparison between the comet image and adjacent field stars. The sky brightness was determined from the median of the pixel values in a concentric annulus with inner and outer radii 10 and 20 pixels (2.″19 and 4.″38), respectively. The magnitudes of the reference field stars were determined by direct comparison with Landolt (1992) standards observed nearby in time and air mass. These measurements were made using circular apertures 4.″38 in radius, with sky determined from an annulus extending from 4.″38 to 6.″57 in radius. We employed standard stars with $m_V - m_R$ colors like that of the Sun in order to minimize the effects of color terms in the photometry. The photometry is given in Table 2.

3. OBSERVATIONAL RESULTS

3.1. *Surface Brightness Profile*

Individual images of 48P from the February, March, and April data appear stellar, with no trace of coma. We shifted and combined sequences of images to search for near-nucleus

TABLE 2
RED-FILTER PHOTOMETRY

No.	UT Date (2003)[a]	m_R[b]	No.	UT Date (2003)[a]	m_R[b]	No.	UT Date (2003)[a]	m_R[b]
1	Feb 25.4785	21.59	33	Mar 4.4980	21.72	65	Apr 1.5732	21.02
2	Feb 25.4846	21.72	34	Mar 4.5039	21.66	66	Apr 1.5782	21.09
3	Feb 25.5198	21.74	35	Mar 4.5098	21.65	67	Apr 1.6068	21.01
4	Feb 25.5257	21.70	36	Mar 4.5158	21.67	68	Apr 1.6121	21.08
5	Feb 25.5820	21.82	37	Mar 4.5217	21.74	69	Apr 1.6175	21.07
6	Feb 25.5880	21.77	38	Mar 4.5276	21.66	70	Apr 1.6402	21.12
7	Feb 25.6373	21.85	39	Mar 4.5850	21.51	71	Apr 2.4745	21.13
8	Feb 25.6432	21.80	40	Mar 4.5909	21.59	72	Apr 2.4799	21.08
9	Feb 26.4817	21.79	41	Mar 4.5969	21.51	73	Apr 2.4853	21.08
10	Feb 26.4876	21.84	42	Mar 4.6028	21.61	74	Apr 2.4907	21.08
11	Feb 26.5328	21.62	43	Mar 4.6087	21.49	75	Apr 2.5170	20.97
12	Feb 26.5433	21.65	44	Mar 4.6147	21.50	76	Apr 2.5223	20.95
13	Feb 26.5872	21.53	45	Mar 4.6206	21.39	77	Apr 2.5278	20.98
14	Feb 26.5932	21.62	46	Mar 4.6265	21.45	78	Apr 2.5498	20.90
15	Feb 26.6374	21.56	47	Mar 4.6304	21.54	79	Apr 2.5664	20.99
16	Feb 26.6427	21.64	48	Mar 5.5286	21.78	80	Apr 2.5719	20.93
17	Mar 2.5587	21.74	49	Mar 5.5345	21.75	81	Apr 3.3425	20.90
18	Mar 2.5635	21.76	50	Mar 5.5404	21.87	82	Apr 3.3468	20.88
19	Mar 2.5683	21.68	51	Mar 5.5466	21.83	83	Apr 3.4380	21.14
20	Mar 2.5732	21.72	52	Mar 5.5790	21.76	84	Apr 3.4427	21.09
21	Mar 2.5781	21.79	53	Mar 5.5849	21.78	85	Apr 3.5016	21.18
22	Mar 2.5832	21.75	54	Mar 5.5909	21.78	86	Apr 3.5064	21.07
23	Mar 2.6208	21.73	55	Mar 5.6224	21.90	87	Apr 3.5113	21.20
24	Mar 2.6481	21.63	56	Mar 5.6283	21.82	88	Apr 3.5596	21.16
25	Mar 3.5766	21.55	57	Mar 5.6343	21.81	89	Apr 3.5638	21.18
26	Mar 3.5814	21.54	58	Apr 1.4827	20.94	90	Apr 3.5997	21.24
27	Mar 3.5862	21.63	59	Apr 1.4886	20.95	91	Apr 3.6050	21.22
28	Mar 3.6299	21.57	60	Apr 1.4945	20.93	92	May 27.3399	21.22
29	Mar 3.6347	21.59	61	Apr 1.5006	20.92	93	Jul 2.3063	21.68
30	Mar 3.6395	21.55	62	Apr 1.5401	21.03	94	Jul 2.3313	21.50
31	Mar 3.6581	21.74	63	Apr 1.5454	20.99			
32	Mar 4.4921	21.73	64	Apr 1.5682	20.96			

[a] Universal Time at the start of each integration.
[b] Apparent red magnitude. The uncertainty on each magnitude is near ±0.05 mag.

coma fainter than visible in individual images. Shifted combinations of data from the UH telescope showed no evidence of coma. A deeper search was enabled by the great light-gathering power of the Keck 10 m telescope. Keck data were also obtained at a smaller heliocentric distance than the bulk of the UH 2.2 m data ($R \sim 3.70$ vs. 4.00 AU), providing an improved sensitivity to faint coma. The most suitable data for a coma search were a set of four *I*-band images each of 150 s integration, with telescope position dithering between images. In Figure 1 (*left*), we show an image formed by combining these four images, each sky-subtracted and shifted to a common center, taken on UT 2003 May 27. The individual images and their combination have 0.″73 FWHM. A very faint tail is evident extending in position angle 130°. In the right panel of Figure 1, we show the result of subtracting a scaled image of a field star, formed by shifting and combining the same four images used to compute the comet image. The subtraction shows no evidence for coma within the image core but emphasizes the tail. The latter is visible at very low surface brightness levels to ∼5″ from the nucleus, where it becomes confused with the images of two faint background galaxies. In surface brightness, the tail is comparable to the systematic errors in the flat-fielding of the data (see, e.g., the dark regions in Fig. 1, *right*) and is, in this sense, immeasurably faint. Since the *I* band includes few bright cometary molecular emission bands, and because 48P is still at considerable heliocentric distance ($R = 3.70$ AU in Fig. 1), it is likely that this is a dust, rather than a plasma, tail.

To assess the near-nucleus coma, the surface brightness profile was computed from the mean signal in a set of annuli centered on the photocenter of the comet image. The profile is compared with the surface brightness of a nearby field star in Figure 2. Note that both profiles are normalized to unity at the center, where the peak surface brightness of the comet is $\Sigma = 19.4$ mag arcsec^{-2}. The profiles of star and comet overlap in the plotted range of radii, p, the difference falling to $\sim 10^{-3}$ of the peak surface brightness at $p \geq 2''$. This corresponds to a coma surface brightness limit $\Sigma_c(2) \geq 26.9$ mag arcsec^{-2}. This value includes the faint tail shown in Figure 1. The fact that the star and comet profiles are indistinguishable emphasizes

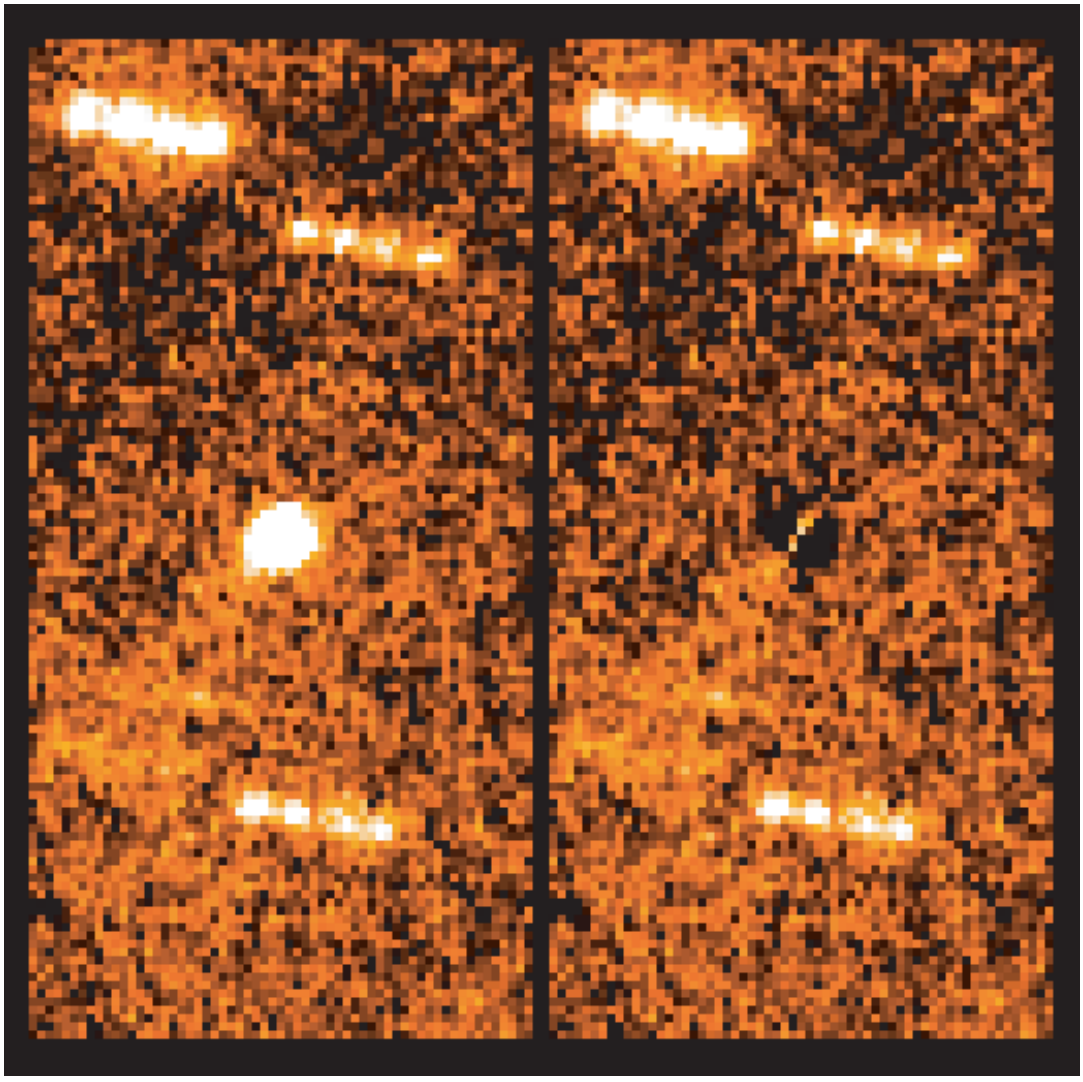

Fig. 1.—*Left*: Image of 48P/Johnson taken at the Keck I Telescope on UT 2003 May 27 and formed from the sum of four *I*-band integrations each of 150 s duration. The images have been shifted to remove the motion of the comet between integrations. The point-spread function of the composite is 0.″73 FWHM. *Right*: Same as the left panel, but with a scaled, aligned image of a star subtracted. Each panel is approximately 12″ × 24″ in size and has north at the top, east at the left. No circumnuclear coma is visible in either panel (see also Fig. 2), but a low surface brightness tail is seen extending to the southeast.

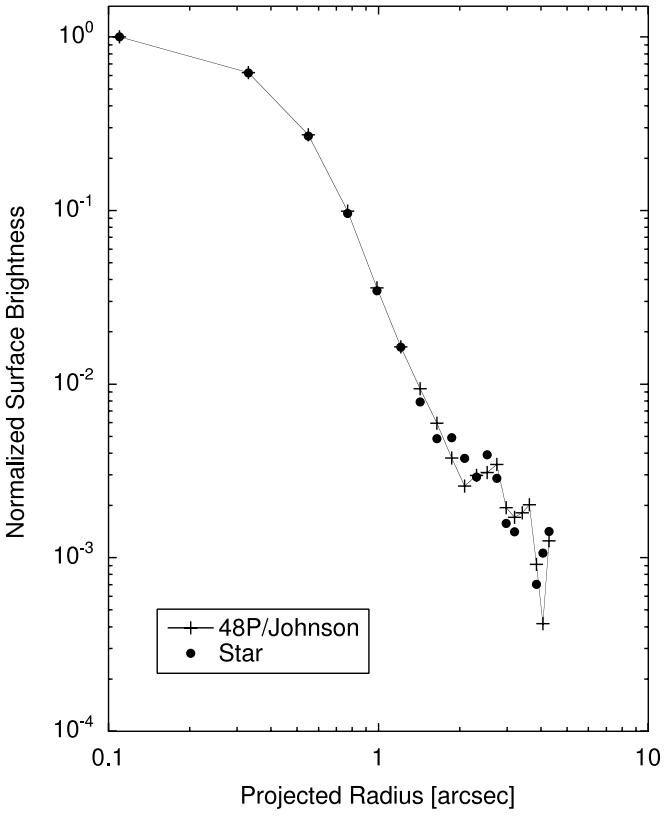

FIG. 2.—Surface brightness profile of comet 48P/Johnson obtained using Keck *I*-band data from UT 2003 May 27. The comet profile is compared with the image point-spread function determined from background stars in the same data. One unit of surface brightness corresponds to $\Sigma(m_R) = 19.4$ mag arcsec^{-2}. The star and comet profiles are indistinguishable within the noise.

the extremely low surface brightness of the latter. At radii $p \geq 4''$, the random effects of noise and the systematic effects of small uncertainties in the sky background become excessive, and the profiles are not well defined.

For a steady state coma (i.e., one in which the volume density of dust grains falls with the inverse square of the distance from the nucleus), the coma surface brightness at radius p (arcseconds) is related to the integrated magnitude measured within radius p, denoted $m_c(p)$, by

$$m_c(p) = \Sigma_c(p) - 2.5 \log 2\pi p^2, \quad (1)$$

where $\Sigma_c(p)$ is the coma surface brightness (mag arcsec^{-2}; Jewitt & Danielson 1984). Substituting $p = 2''.0$ and $\Sigma_c(2) \geq 26.9$ mag arcsec^{-2} (Fig. 2), we obtain $m_c(2) \geq 23.4$ mag. The integrated magnitude of the comet is measured to be $m_I = 20.83 \pm 0.04$, meaning that steady state coma can contribute a fraction less than $10^{0.4[m_I - m_c(2)]} \sim 0.10$ of the total light from 48P.

3.2. *Period and Shape*

The magnitude of 48P/Johnson reduced to unit heliocentric and geocentric distances, $m_R(1, 1, \alpha) = m_R(\alpha) - 5 \log R\Delta$, rises or falls within each night of observation by an amount larger than the measurement error. This suggests rotation of the nucleus with a period longer than the typical nightly time span. Superposed on these internight variations is a longer term trend in the brightness of the comet caused by changes in the Sun-comet-Earth geometry. We sought to determine the light-curve period using phase dispersion minimization (PDM). In this method, the rotational phase is calculated for a given assumed period and the dispersion in the phase-binned data is used as a metric of the quality of the best-fit period (Stellingwerf 1978). The minimum dispersion is taken to reflect the true periodicity in the data. The PDM analysis is summarized in Figure 3. There are several local minima in the plot. Those separated in frequency by 1 day^{-1} are aliases induced by the nightly sampling of the comet. The deepest minimum occurs at

$$P_1 = 14.50 \pm 0.02 \text{ hr}, \quad (2)$$

which we take to be the best estimate of the light-curve period (a comparably deep minimum near 1.2 day^{-1} does not give an acceptable light curve in the phased data). The uncertainty on this period was estimated from an examination of the degradation of the phase plot as the period is changed about the best-fit value. Whether this is also the rotation period of the nucleus depends on the cause of the observed brightness variations. If albedo spots are responsible, then we may directly identify the single-peaked light-curve period P_1 with the rotation period. If, instead, the light curve is caused by a rotational variation of the geometric cross section (i.e., the nucleus is elongated), then the light curve should be double peaked, corresponding to rotation period

$$P_2 = 29.00 \pm 0.04 \text{ hr}. \quad (3)$$

From experience with other cometary nuclei, in which photometric light curves are clearly associated with elongated shape, we suspect that the true rotation period is $P_2 = 29.00 \pm 0.04$ hr. A comparison of the phase plots (Figs. 4 and 5) for P_1 and P_2 shows that the P_2 curve has less scatter at a given rotational phase than does the P_1 curve, and that the former shows distinctly unequal maxima that are best explained as being due to rotation of a pear-shaped body. Unfortunately, the long period of 48P means that the rotational phase plot for P_2 is less filled than that for P_1 and therefore less visually impressive. Still, we identify P_2 with the likely rotation period of the nucleus.

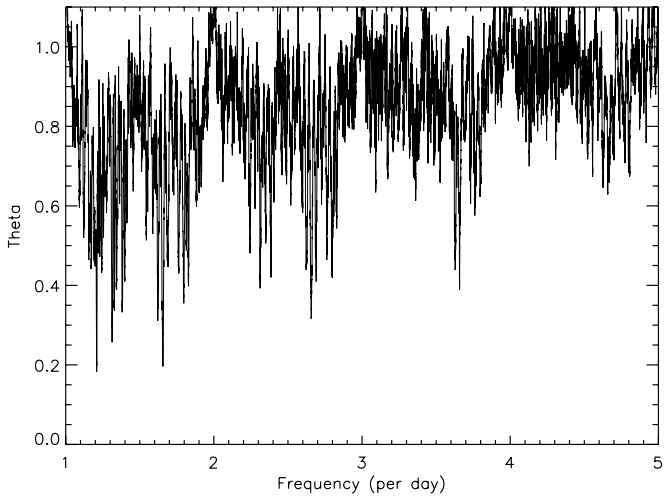

FIG. 3.—Phase dispersion minimization curve for the 48P/Johnson *R*-band data. Here Θ is a normalized measure of the binned dispersion, as defined by Stellingwerf (1978).

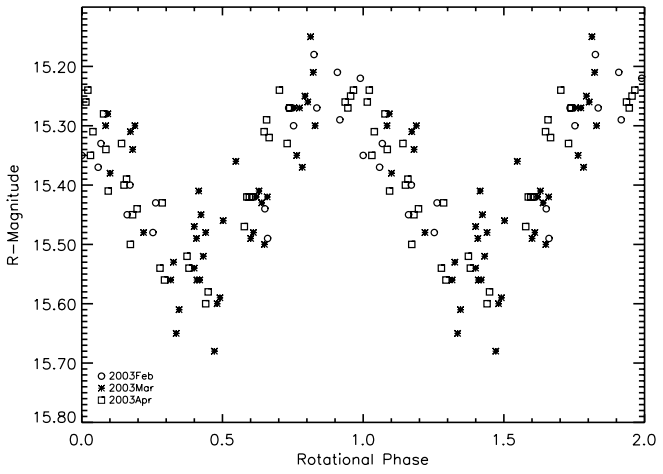

FIG. 4.—Light curve of 48P/Johnson phased to a common period $P_1 = 14.498$ hr. The light curve is singly periodic, consistent with being caused by albedo spots on the nucleus.

The peak-to-peak range of the light curve is $\Delta m_R = 0.32 \pm 0.05$ mag. If due to shape, this corresponds to an axis ratio $b/a = 10^{-0.4\Delta m_R}$, or

$$b/a = 0.74 \pm 0.03 \quad (4)$$

when projected into the plane of the sky. This is a lower limit to the intrinsic axis ratio that would be observed in the absence of projection.

3.3. *Size and Phase Function*

To examine the phase function of the comet, we used the rotational light curve from § 3.2 to correct $m_R(1, 1, \alpha)$ for the rotational modulation. The resulting reduced magnitudes are plotted against phase angle, α, in Figure 6, with error bars that are the 1 σ standard deviations on the nightly means. Figure 6 shows that the mean reduced magnitude of the comet varies with the phase angle of observation, consistent with the effects of phase darkening.

The data are well matched by a phase law in which the magnitude of the comet varies as

$$m_R(\alpha) = m_R(1, 1, 0) + 5 \log R\Delta + \beta\alpha, \quad (5)$$

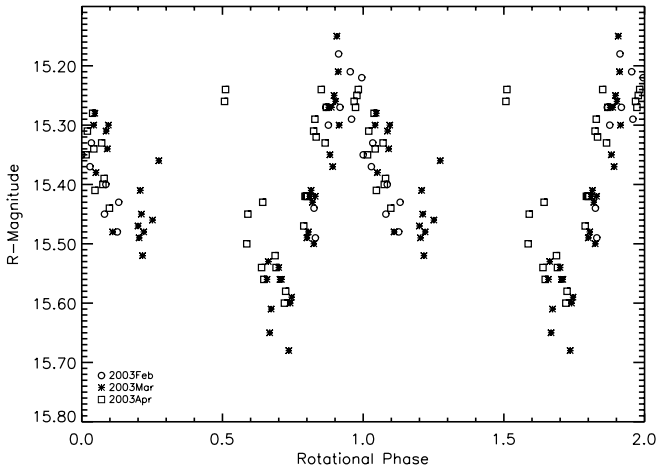

FIG. 5.—Light curve of 48P/Johnson phased to a common period $P_2 = 28.996$ hr. The light curve is doubly periodic, consistent with being caused by rotation of an elongated nucleus.

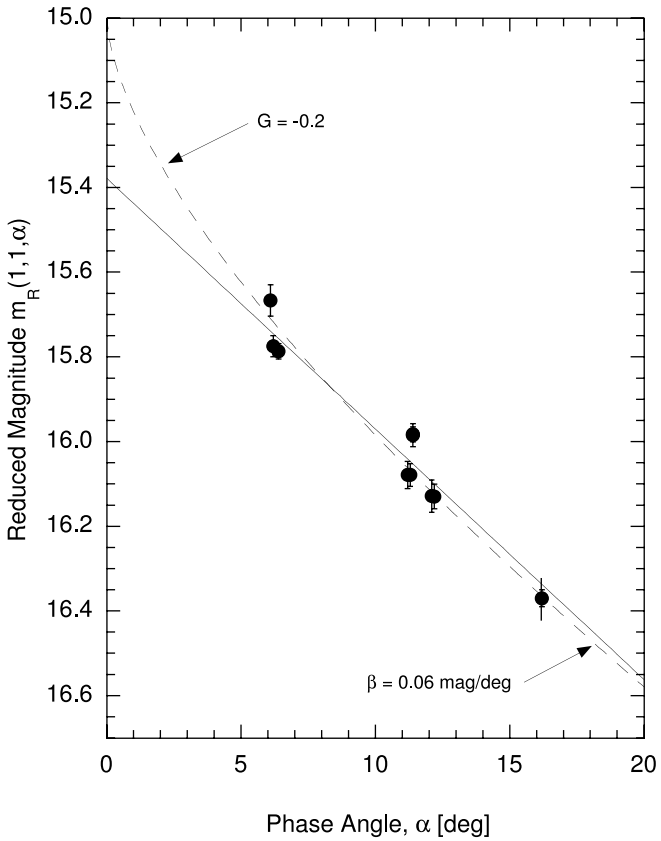

FIG. 6.—Mean magnitude of 48P/Johnson reduced to unit heliocentric and geocentric distances and plotted as a function of the phase angle of observation. The solid line through the data shows the linear phase function $\beta = 0.059$ mag deg^{-1}, while the dashed line shows a Bowell-Lumme-Harris type phase law with $G = -0.2$.

where R and Δ are the heliocentric and geocentric distances in AU, α is the phase angle in degrees, and β (mag deg^{-1}) is the linear phase coefficient. The quantity $m_R(1, 1, 0)$ is the so-called absolute magnitude of the nucleus, equal to the magnitude that would be measured at unit R and Δ and at 0° phase angle. A weighted least-squares fit gives $m_R(1, 1, 0) = 15.38 \pm 0.03$ mag and $\beta = 0.059 \pm 0.002$ mag deg^{-1}. For comparison, Tancredi et al. (2000) used the magnitude compilation by Kamel (1992) to estimate a reduced V-band nuclear magnitude for 48P of $m_V(1, 1, 0) = 15.9$, which we consider to be in good agreement with our R-band measurements. The phase functions are known for a handful of other comets, including 2P/Encke ($\beta = 0.06$ mag deg^{-1}; Fernández et al. 2000), 19P/Borrelly ($\beta = 0.05$ mag deg^{-1}; Soderblom et al. 2002), 28P/Neujmin 1 ($\beta = 0.025 \pm 0.006$ mag deg^{-1}; Delahodde et al. 2001), and 143P/Kowal-Mrkos ($\beta = 0.043 \pm 0.014$ mag deg^{-1}; Jewitt et al. 2003). The nucleus of 48P/Johnson does not stand out in the context of these measurements.

As an alternative representation of the phase function, we compared the data in Figure 6 with the "*H-G*" model advocated by the IAU (Bowell et al. 1989). One sample curve, with $G = -0.2$, is shown for comparison in the figure. The *H-G* model fits the data equally well but includes an opposition surge of about 0.3 mag above the extrapolation of the linear relation. Since we do not know the small phase angle behavior of the scattering from 48P, we must regard this as an important source of uncertainty. Accordingly, we conclude that the absolute magnitude is not fainter than given by the linear phase

coefficient but might be considerably brighter. We adopt the midpoint of the linear and $G = -0.2$ extrapolations,

$$m_R(1, 1, 0) = 15.23 \pm 0.10, \quad (6)$$

as our best estimate of the absolute magnitude.

In the absence of an independent measurement of the albedo of the nucleus, we cannot determine the radius of the nucleus from our data. However, measurements of other nuclei show that the albedos are all small, with $p_R = 0.04$ being a useful mean. Adopting this value for 48P/Johnson, we estimate an effective circular radius

$$r_e = 2.6 \pm 0.2 \text{ km}. \quad (7)$$

This is compatible with the upper limit obtained by Lowry & Fitzsimmons (2002), $r_e \leq 3.5$ km (albedo 0.04 again assumed), from observations taken in the presence of coma. For comparison, the effective radius of the nucleus of 1P/Halley is $r_e \sim 5$ km (Keller et al. 1987), and that of 19P/Borrelly is $r_e = 3$ km (Soderblom et al. 2002). We note that Belskaya & Shevchenko (2000) have reported an empirical inverse correlation between the phase function and the V-band geometric albedo, p_V. Their reported correlation and the large phase effect in 48P are together consistent with our assumption of a low albedo.

Lastly, keeping in mind the picture of the nucleus as an ellipsoid, the semiaxes projected into the plane of the sky are

$$a \times b = 3.0 \times 2.2 \text{ km}. \quad (8)$$

The asymmetric light curve (Fig. 5) suggests that this ellipsoid is further distorted into a pear shape.

4. DISCUSSION

In the modern paradigm, the Jupiter-family comets are escaped from the Kuiper belt and have spent perhaps $\sim 10^7$ yr (the median lifetime) in the transitional Centaur phase (Tiscareno & Malhotra 2003). Observations of other JFC nuclei suggest that these objects have been substantially processed since their injection into the region of the terrestrial planets. Their surfaces are depleted in the "ultrared" matter that is a prominent feature of many of the Kuiper belt objects and Centaurs (Jewitt 2002). Their nuclei are too elongated to have been shaped only by collisional fragmentation of Kuiper belt parents (Jewitt et al. 2003), while the timescales for outgassing torques to excite the nucleus spin are so short that the current rotations of these bodies are not likely to be primordial.

The nucleus of 48P/Johnson is set in the context of other well-measured JFC nuclei in Figure 7. Period versus photometric range data in the figure are taken from Table 4 of Jewitt et al. (2003). The plotted nuclei have all been measured photometrically, by the same technique as used in the present paper. For comparison, we also plot period versus range data for a complete sample of small main-belt asteroids (SMBAs) taken from Binzel et al. (1992). (Note that we have omitted asteroid 29196 [1990 YY] from the Binzel et al. compilation because it is an L5 Trojan rather than a main-belt asteroid.) The SMBAs are included as an example of a highly collisionally processed population.

Solid lines in Figure 7 mark the centripetal limits for assumed densities ρ of 250, 500, 1000, and 2000 kg m^{-3}, computed from equations (7) and (8) of Jewitt & Meech (1988). The measured nuclei are all rotationally stable for densities $\rho \geq 500$ kg m^{-3}, whereas the most rapidly rotating SMBAs require $\rho \geq 2000$ kg m^{-3} to resist centripetal breakup in the absence of

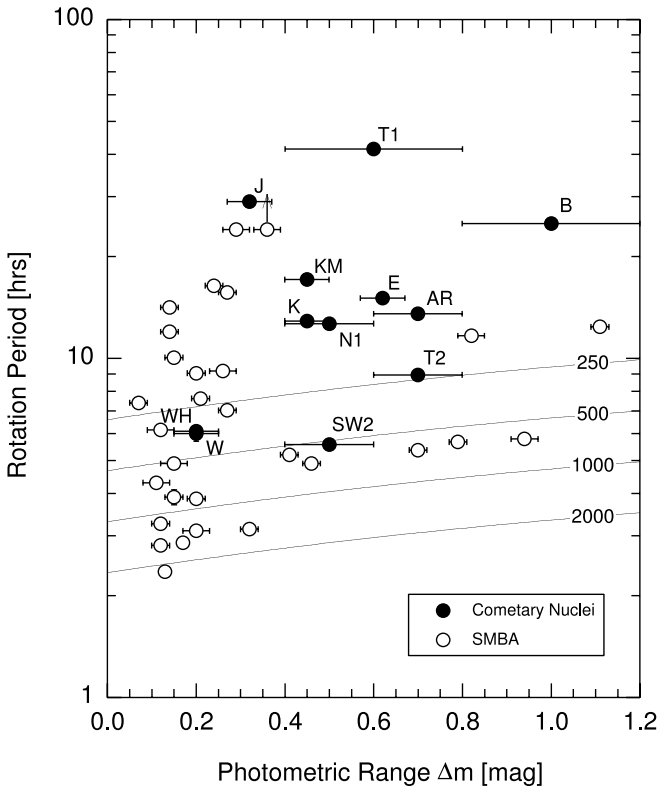

FIG. 7.—Photometric range vs. rotation period for the JFC nucleus sample (*filled circles*) and for small main-belt asteroids (*open circles*) from Binzel et al. (1992). The labeled lines mark stability trajectories computed as described in the text for densities ρ of 250, 500, 1000, and 2000 kg m^{-3}. Individual nuclei marked are 49P/Arend-Rigaux (AR), 19P/Borrelly (B), 2P/Encke (E), 48P/Johnson (J), 22P/Kopff (K), 143P/Kowal-Mrkos (KM), 28P/Neujmin 1 (N1), 31P/Schwassmann-Wachmann 2 (SW2), 9P/Tempel 1 (T1), 10P/Tempel 2 (T2), 46P/Wirtanen (W), and 107P/Wilson-Harrington (WH).

significant tensile strength. This is relevant because observations strongly suggest that asteroids larger than ~ 150 m in diameter possess negligible tensile strength, presumably as a result of an internally fractured composition (Pravec, Harris, & Michalowski 2002). The internal structure of the comets is unknown, but the breakup of D/Shoemaker-Levy 9 inside the Roche sphere of Jupiter independently suggests a very low tensile strength (Asphaug & Benz 1996). Therefore, the absence of very rapidly rotating comets in Figure 7 may be telling us that the nuclei of JFCs are low in both tensile strength and density: nuclei that have been driven above the centripetal limit by outgassing forces are missing from the figure because they have been destroyed. The nucleus of 48P, in contrast, is one of the most slowly rotating of the measured nuclei.

Figure 7 shows that the JFC nuclei have a mean photometric range ($\overline{\Delta m_R} = 0.52 \pm 0.07$ [$N = 12$]) that is systematically larger than the mean range of the SMBAs ($\overline{\Delta m_R} = 0.31 \pm 0.05$ [$N = 32$]), as already noted by Jewitt & Meech (1988) and Jewitt et al. (2003). Judged by the Kolmogorov-Smirnov test, the difference in the range distributions is significant at the 99.6% (3 σ) confidence level. We believe this difference to be caused by prolonged, nonuniform mass loss from the JFC nuclei. The figure also suggests that the mean rotational period of the JFC nuclei ($\bar{P} = 16.1 \pm 3.1$ hr [$N = 12$]) is larger than the mean period of the SMBAs ($\bar{P} = 8.3 \pm 1.1$ hr [$N = 30$]), but this effect is significant only at the 98.3% (2.5 σ) level according to the Kolmogorov-Smirnov

test. There is reason to think that the significance of the period difference may be even smaller, since two SMBAs having indeterminate (but probably very long [≫24 hr]) periods were not included in Figure 7 or in the Kolmogorov-Smirnov test.

In the 15 years since the period versus shape relation for cometary nuclei was first examined (cf. Fig. 7 here with Fig. 7 of Jewitt & Meech 1988), the basic physical characterization of these objects has changed relatively little. In contrast, our thoughts about the processes that have shaped the nuclei and influenced their spins are completely different. In 1988, it was possible to entertain the belief that the shapes of the nuclei might reflect the conditions of accretion, whereas now their integrated mass loss is seen to be so large that the shapes can hardly be primordial (Jewitt et al. 2003). The spins, likewise, were thought by many to reflect the initial complement of angular momentum delivered at accretion but now are seen to be determined by torques due to asymmetric mass loss. Cometary nuclei may still retain primordial compositional characteristics, but their physical properties are evidently highly modified.

5. SUMMARY

Time-resolved observations of Jupiter-family comet 48P/Johnson near heliocentric distance $R = 4$ AU show the following:

1. The surface brightness profile is pointlike, limiting the fraction of the light that is scattered by unresolved, steady state coma to $\leq 10\%$.

2. The brightness of the comet varies cyclically with time, which we interpret to be a result of rotation of the comet nucleus. If the light curve has two maxima per period, as expected for an elongated body, the preferred period is 29.00 ± 0.04 hr. The light curve shows a $\Delta m_R = 0.32 \pm 0.05$ mag peak-to-peak range. This corresponds to a nucleus axis ratio $b/a = 0.74 \pm 0.03$ when projected into the plane of the sky (this is a lower limit to the intrinsic axis ratio).

3. Phase-angle–dependent variations in the apparent brightness of 48P/Johnson are compatible with a linear coefficient $\beta = 0.059 \pm 0.002$ mag deg^{-1}. This large phase coefficient, in turn, is consistent with (but does not require) a low-albedo surface.

4. The absolute magnitude of the nucleus is $m_R(1, 1, 0) = 15.23 \pm 0.10$. If the red geometric albedo is $p_R = 0.04$, the effective circular radius of 48P/Johnson is $r_e = 2.6 \pm 0.2$ km, but the true shape is closer to a 3.0×2.2 km ellipsoid.

We are grateful to telescope operators John Dvorak and Paul deGrood. This work was supported by a grant to D. J. from the NASA Planetary Astronomy Program.

REFERENCES

Asphaug, E., & Benz, W. 1996, Icarus, 121, 225
Belskaya, I. N., & Shevchenko, V. G. 2000, Icarus, 147, 94
Binzel, R. P., Xu, S., Bus, S. J., & Bowell, E. 1992, Icarus, 99, 225
Bowell, E., Hapke, B., Domingue, D., Lumme, K., Peltoniemi, J., & Harris, A. W. 1989, in Asteroids II, ed. R. P. Binzel, T. Gehrels, & M. S. Matthews (Tucson: Univ. Arizona Press), 524
Carusi, A., Kresák, L., Perozzi, E., & Valsecchi, G. B. 1985, Long-Term Evolution of Short-Period Comets (Bristol: Hilger), 50
Delahodde, C. E., Meech, K. J., Hainaut, O. R., & Dotto, E. 2001, A&A, 376, 672
Fernández, Y. R., et al. 2000, Icarus, 147, 145
Jewitt, D., Sheppard, S., & Fernández, Y. 2003, AJ, 125, 3366
Jewitt, D. C. 2002, AJ, 123, 1039
Jewitt, D. C., & Danielson, G. E. 1984, Icarus, 60, 435
Jewitt, D. C., & Meech, K. J. 1988, ApJ, 328, 974
Johnson, E. 1949, IAU Circ. 1228
Kamel, L. 1992, A&AS, 92, 85
Keller, H. U., et al. 1987, A&A, 187, 807
Landolt, A. U. 1992, AJ, 104, 340
Lowry, S. C., & Fitzsimmons, A. 2001, A&A, 365, 204
Oke, J. B., et al. 1995, PASP, 107, 375
Pravec, P., Harris, A. W., & Michalowski, T. 2002, in Asteroids III, ed. W. F. Bottke, A. Cellino, P. Paolicchi, & R. P. Binzel (Tucson: Univ. Arizona Press), 113
Soderblom, L. A., et al. 2002, Science, 296, 1087
Stellingwerf, R. F. 1978, ApJ, 224, 953
Tancredi, G., Fernández, J. A., Rickman, H., & Licandro, J. 2000, A&AS, 146, 73
Tiscareno, M. S., & Malhotra, R. 2003, AJ, 126, 3122